Field-effect density modulation in Si nanowires for increasing *ZT*: A simulation study

Neophytos Neophytou[1], Hossein Karamitaheri[2], and Hans Kosina[3]

[1]School of Engineering, University of Warwick, Coventry, CV4 7AL, UK

[2]Department of Electrical Engineering, University of Kashan, Kashan, 87317-51167, Iran

[3]Institute for Microelectronics, Technical University of Vienna, Austria

email: N.Neophytou@warwick.ac.uk

Abstract

Modulation doping is a promising way to increase the electronic conductivity of thermoelectric materials and achieve high *ZT* figure of merit. In this work we provide a qualitative and quantitative comparison of the thermoelectric performance of a field-effect density modulated Si nanowire channel of diameter *D*=12nm versus its doped counterpart. We employ self-consistent atomistic tight-binding simulations coupled to the Boltzmann transport equation. We describe the simulation model, and show that as a result of a large improvement in the electrical conductivity, gating, rather than doping, can provide improvements on the thermoelectric power factor larger than 3x. Despite the large increase in the electronic part of the thermal conductivity, the total thermal conductivity is still dominated by phonons. Thus, a *ZT* figure of merit more than 3x higher can be achieved in the gated channel compared to the doped channel as well. Finally, we show that similar to the case of doped channels, the power factor peak is obtained when the Fermi level resides ~k_BT below the band edge.

Index terms: silicon nanowires, low-dimensional thermoelectrics, gated thermoelectrics, Boltzmann transport, thermoelectric power factor, Seebeck coefficient

I. Introduction

The ability of a thermoelectric material to convert heat into electricity is quantified by the dimensionless figure of merit $ZT=\sigma S^2T/\kappa$, where σ is the electrical conductivity, S is the Seebeck coefficient, and κ is the thermal conductivity. Nanostructured and low-dimensional silicon based thermoelectric (TE) materials have demonstrated large performance enhancement compared to the bulk material because of a large reduction in their thermal conductivity due to strong phonon-boundary scattering. The *ZT*, however, could be further improved by increases in the power factor. The power factor peaks at high concentrations around 10^{19}-10^{20}/cm^3, and in most cases this is achieved by doping. Doping at such high levels, however, introduces strong ionized impurity scattering (IIS) on charged carriers, and severely limits mobility and electronic conductivity. In an earlier work we compared the phonon-limited to the phonon plus IIS thermoelectric power factor in Si nanowires (NWs) and demonstrated that both the power factor and *ZT* could be more than a factor of ~3x lower in the presence of IIS [1]. Thus, modulation doping has been suggested as a possible way to achieve the required high carrier densities, but without the detrimental effects of the ionized dopants in the channel [2]. Indeed, several experimental works indicated that thermoelectric performance modulation over orders of magnitude can be achieved using modulation doping techniques, but in all cases the improvement was only modest [2, 3, 4, 5, 6, 7, 8].

In this work we examine theoretically the performance of the gated versus the doped Si nanowire channel in order to qualitatively and quantitatively identify the benefits that can be achieved by modulation doping. The choice of Si nanowire channel is due to the fact that nanowires have demonstrated significant *ZT* enhancements as a result of a large reduction in their thermal conductivity, which reached values as low as κ=1-2 W/mK [9, 10]. We theoretically evaluate the additional performance improvement that can result from the power factor using gating. We employ self-consistent atomistic tight-binding calculations couple to Boltzmann transport equation. We show that remarkable power factor and *ZT* improvements larger than 3x can be achieved in gated channels.

II. Method

The complete computational model is described in Fig. 1. There are four steps in the computation [11]:

i) The first step is the calculation of the electronic bandstructure of the nanowire channel using the $sp^3d^5s^*$ tight-binding (TB) atomistic model [12, 13, 14]. The Schrodinger equation is solved only in the Si channel, whereas the oxide is only included in the electrostatics of the device. The TB model assumes hydrogen passivated edge atoms using an effective passivation scheme described in Ref. [15]. Effectively, this scheme places hard wall boundary conditions on the edge atoms of the channel, while removing all dangling bonds that remain from the unsaturated atomic bonds. This mimics Hydrogen passivation, although there are no actual Hydrogen atoms used in the Hamiltonian construction.

ii) The second step involves the calculation of the charge density using equilibrium statistics. The *k*-states of the bandstructure are filled according to the Fermi level, which is assumed to be uniform along the length of the device. The position of the Fermi level determines the charge density.

iii) The third step is the solution of a 2D Poisson equation in the cross section of the NW. A gate all around geometry is used, with 1.1nm SiO_2 as the gate insulator. When solving the Poisson equation we include the carrier distribution in the channel (as indicated in Fig. 1), which is determined by the coefficients of the eigenvectors of the various *k*-states. These first three steps are solved self-consistently since the bandstructure is a function of the potential profile in the channel. iv) Once self-consistency is achieved, we use the linearized Boltzmann transport formalism to extract the thermoelectric coefficients including all relevant scattering mechanisms, i.e. acoustic phonons, optical phonons, surface roughness scattering (SRS), and ionized impurity scattering (IIS) as described in detail in Refs. [1, 11]. IIS is only applied for doped/non-gated structures. We perform the above procedure for a series of gate biases, driving the channel from depletion to accumulation.

Within the linearized Boltzmann transport theory, the electrical conductivity, Seebeck coefficient, and the electronic part of the thermal conductivity are given by the following expressions:

$$\sigma = q_0{}^2 \int_{-\infty}^{E_0} dE \left(-\frac{\partial f_0}{\partial E} \right) \Xi(E), \tag{1a}$$

$$S = \frac{q_0 k_{\mathrm{B}}}{\sigma} \int_{-\infty}^{E_0} dE \left(-\frac{\partial f_0}{\partial E} \right) \Xi(E) \left(\frac{E - E_F}{k_{\mathrm{B}} T} \right), \tag{1b}$$

$$\kappa_0 = k_B{}^2 T \int_{-\infty}^{E_0} dE \left(-\frac{\partial f_0}{\partial E} \right) \Xi(E) \left(\frac{E - E_F}{k_B T} \right)^2, \tag{1c}$$

$$\kappa_e = \kappa_0 - T\sigma S^2. \tag{1d}$$

The energy E integration over the derivative of the Fermi distribution $f_0(E)$ is performed from the valence band edge E_0 though all energies. $\Xi(E)$ is the transport distribution function (TD) defined as [1, 16, 17]:

$$\begin{aligned} \Xi(E) &= \frac{1}{A} \sum_{k_x, n} v_n{}^2 (k_x) \tau_n (k_x) \delta \left(E - E_n (k_x) \right) \\ &= \frac{1}{A} \sum_n v_n{}^2 (E) \tau_n (E) g_{1D}^n (E). \end{aligned} \tag{2}$$

Here $v_n(E) = \frac{1}{\hbar} \frac{\partial E_n}{\partial k_x}$ is the bandstructure velocity of subband n with dispersion E_n, $\tau_n(k_x)$ is the momentum relaxation time for a carrier with wavenumber k_x in subband n,

$$g_{1D}^n (E) = \frac{1}{2\pi\hbar} \frac{1}{v_n (E)} \tag{3}$$

is the density of states for the 1D subbands (per spin), and A is the cross sectional area of the NW.

For SRS we assume a 1D exponential autocorrelation function for the roughness, with roughness amplitude Δ_{rms} = 0.48nm and roughness correlation length L_{C} =1.3nm [18]. In the case of doped nanowires, with a flat potential in their cross section, surface roughness is assumed to cause a band edge shift due to diameter modulation. The

scattering strength is derived from the shift in the band edge with quantization $\frac{\Delta E_0}{\Delta D}$ [19, 20], and the transition rate here is given as:

$$S_{n,m}^{SRS}(k_x,k_x') = \frac{2\pi}{\hbar}\left(\frac{q_0\Delta E_0}{\Delta D}\right)^2\left(\frac{2\sqrt{2}\Delta_{rms}{}^2 L_C}{2+q_x{}^2 L_C{}^2}\right)\delta\left(E_m(k_x')-E_n(k_x)\right), \qquad (4)$$

where $q_x = k_x - k_x'$. The band edge variation is the dominant SRS mechanism in ultra scaled channels and results in the low-field mobility in ultra thin nanostructures to follow a D^6 behavior, where D is the confinement length scale, in this case the diameter of the channel. Note, however, that for D>10nm, this effect is weak. In addition, for NWs with flat potential in their cross section, in which case transport mostly happens within the NW core, SRS is in general weak.

For SRS in the gated NWs, we follow the usual way of deriving the scattering matrix element and scattering rates from the strength of the radial electric field in the channel [21]. The transition rate is given by:

$$S_{n,m}(k_x,k_x') = \frac{2\pi}{\hbar}\left|\left\langle F_f\left|\mathcal{E}_{eff}(r)\right|F_i\right\rangle\right|^2\frac{\Delta_{rms}^2 L_C}{\left(2+q_x^2L_C^2\right)}\delta\left(E_m(k_x')-E_n(k_x)\right) \qquad (5)$$

Above, $\delta(\square)$ is the Dirac-delta function which denotes energy conservation, $F_{f,i}$ are the final/initial bound states in the transverse plane (NW cross section), $\mathcal{E}_{eff}$ is the radial gate-induced electric field in the NW cross section, and $q_x = k_x - k_x'$.

III. Results

The required charge density for high thermoelectric power factor is around 10^{19}/cm^3-10^{20}/cm^3. The advantage in achieving such high carrier concentration by gating rather than doping, lies in the fact that ionized impurity dopants will significantly reduce the electrical conductivity [22]. Figure 2a compares the electrical conductivity versus carrier concentration of the [100] NW with diameter D=12nm for these two channels.

Three cases are depicted: i) Gated NW with phonon-limited scattering transport considerations (blue-dot-solid line); ii) Gated NW with phonon scattering and SRS transport considerations (blue-dot-dashed line); iii) Doped NW with phonon scattering, SRS, and IIS transport considerations (black-solid line). Due to the absence of ionized impurity scattering, the electrical conductivity of the gated channel largely surpasses that of the doped channel. An important point to be mentioned here is that including SRS on top of phonon scattering affects the conductivity of the gated channel only to a small degree, and that only at concentrations above $p = 3\text{x}10^{19}/\text{cm}^3$ (dashed versus solid blue-dot lines). In the case of the doped channel, where IIS (and SRS) is additionally considered in the calculations, the conductivity significantly drops. Figure 2b shows the Seebeck coefficient of the same channel for the same cases as described above. The Seebeck coefficient, following the reverse trend compared to the conductivity, is larger in the case of the doped channel, but degraded in the case of the gated NW (blue-dot-solid line versus black-solid line).

The magnitude of the degradation in the Seebeck coefficient, however, is not significant compared to the increase in the electrical conductivity in the absence of doping. Note that a relatively small change in the Seebeck coefficient between direct doping and modulation doping was also observed experimentally in Ref. [2]. As a result of the superior conductivity, the thermoelectric power factor shown in Fig. 3 is much larger in the case of the gated channel compared to the doped channel. The power factor of the gated channel peaks at concentrations around $p \sim 10^{19}/\text{cm}^3$, and it is more that 3x higher compared to that of the doped channel. This qualitatively and quantitatively demonstrates the advantage of the gated NW channels for achieving large thermoelectric power factors compared to the traditionally used doped materials. It is again interesting to observe that SRS degrades the power factor of the gated channel only slightly (blue-dashed-dot line). On the other hand, IIS is already strong enough at this concentration to cause significant degradation to the power factor of the doped channel (black-solid line). It is also interesting to notice the sharp peak in the power factor of the gated channel, compared to the smooth peak in the case of the doped channel. The reason for the sharp peak is the non-uniform reduction in the Seebeck coefficient of the gated channel for

carrier concentrations above $p \sim 5\text{x}10^{18}/\text{cm}^3$ as shown in Fig. 2b (sharper drop in comparison to the straight-dashed line). At those carrier densities (with $V_G \sim -0.4\text{V}$), the accumulation layer starts to form around the surface of the NW, where a potential well is formed. Within the quantum well the bands of the electronic structure of the NW are split in energy, the density of states around the NW circumference thus drops, and the band edge is pushed closer to the Fermi level, compared to what a rigid/pristine electronic bandstructure (in the absence of any electrostatic potential) would do. This results is a sharper drop in the Seebeck coefficient, and a sharper peak in the power factor. From the design point of view, therefore, one needs to be able to dope the NW with relatively high precision to achieve maximum results.

A few experimental works can be found in the literature, which consider the TE performance of inversion layers for various geometries (mostly on much larger geometries, and/or materials other than just Si). Reference [4], for example, measured the power factor of gated n-type nanowires to saturate at high gate biases from around ~1.86 mW/mK^2 to ~2.28 mW/mK^2, depending on the NW dimensions, at carrier densities $\sim 10^{19}/\text{cm}^3$. These values are similar to what we report in this work, however the power factor of n-type Si NWs is expected to be somewhat higher compared to p-type Si NWs [1]. Reference [23] reported measurements and simulations for the power factor in gated p-type Si (110)/[110] nanoribbons of thickness 20nm. The power factor reached a maximum value of ~5 mW/mK^2 for carrier concentrations $\sim 2.5\text{x}10^{19}/\text{cm}^3$. The (110)/[110] channel is known to have superior properties compared to the p-type [100] channel [24], which justifies the higher performance reported compared to the results in Fig. 3. The relative improvement of that gated channel compared to the doped channel, however, was comparable to the results we report for [100] NWs in this work. Reference [2] presents results for a p-type modulation-doped bulk-like SiGe-based system at carrier concentrations of $2.61\text{x}10^{20}/\text{cm}^3$. At 300K, the power factor was measured to be ~ 2.1 mW/mK^2. This was significantly higher compared to the directly doped material ~1.3 mW/mK^2. The improvement in the power factor was a result of the improvement in the conductivity of the material, similar to what we show in this work. Only a limited change in the Seebeck coefficient between direct doping and modulation doping was observed,

as we also see in this work. Finally, reference [6] reported measurements of the power factor in gated p-type Ge-Si core-shell NWs of overall diameters from 15.4nm to 28nm. The power factor reached maximum values varying from ~1 mW/mK^2 up to ~3.6 mW/mK^2 for carrier concentrations ~$5x10^{19}/cm^3$. These values are comparable to what we report, although it is expected that the Si-Ge system will have higher power factors. In all these works, although the amplitude of the power factor can quantitatively vary, improvements were qualitatively demonstrated. The relative power factor increases were somewhat lower than what we theoretically predict, which indicates that there is still room for improvement by proper design and optimization of the experimental channels.

Another important point to stress in Fig. 3 is the fact that SRS does not actually affect the results. The reason why SRS is weak is that the electric field to achieve a hole *accumulation* layer is relatively weak. The electrostatic potential energy across the diameter of the D=12nm NW channel for three different gate bias cases is indicated in Fig. 4. The blue-solid line shows the potential energy in a line coincidental with a NW diameter at V_G = -0.5V, which is the bias for which the power factor maximum is achieved (carrier concentrations p~$10^{19}/cm^3$). For reference, in green-dashed-dot line we show the potential energy under gate bias V_G = -0.4V, which is just before the power factor maximum. In red-dashed line we also show the potential energy under gate bias V_G = -0.6V, which is just after the power factor maximum. The valence band edges are shown by the horizontal lines drawn by the same line forms, respectively. The Fermi level E_F is depicted by the black line. As the gate bias increases (in absolute values), and the channel is driven more into accumulation, the band edges move above the minimum of the potential (located in the center), indicating that the charge is accumulated into the quantum wells formed around the surface of the wire. The valence band edge gets closer to the Fermi level as the $|V_G|$ increases. An interesting point is that the power factor is maximized when the distance of the band edges from the Fermi level is $\eta_F = E_F - E_V \sim k_B T$, as indicated in Fig. 4. This is very similar to what is observed for doped channels as well as described in Ref. [1]. Such η_F value is small enough to provide large conductivity, but large enough to keep the Seebeck coefficient high, which leads to optimized power factors. Another observation is that for the biases above the optimal power factor, the

accumulation layer screens that inner part of the channel such that the potential energy does not shift (upwards) as the bias $|V_G|$ increases. The contribution of the inner pat of the NW to the power factor is limited as the bands in that part are placed further away from the Fermi level. This means that for NW channels with larger diameters in which case the inner part takes a larger part of the volume, the performance could be degraded (since only the outer shell would contribute to high power factors). In any case, nanowires of larger diameters might not be as efficient thermoelectrics because of larger thermal conductivities.

From Fig. 4, the electric field at the surface of the NW for the optimal power factor case V_G = -0.5V, can be deduced to be $\mathcal{E}_{eff}(r = D/2) = 0.19\ \mathrm{MV/cm}$. This value is smaller compared to the electric field needed to achieve an *inversion* layer, as for example in transistor devices. In that case the field is $\mathcal{E}_{eff} > 0.3\ \mathrm{MV/cm}$ [25]. SRS begins to become detrimental to the conductivity for even larger fields, $\mathcal{E}_{eff} > 0.4\ \mathrm{MV/cm}$. In the case of gated thermoelectric channels, therefore, SRS is weak. Note that in the calculation of the SRS rates, we have even used relatively large roughness amplitude values of Δ_{rms} = 0.48nm and correlation lengths L_C = 1.3nm [18].

In order to compute the *ZT* figure of merit, we need to calculate the thermal conductivity as well. The total thermal conductivity is composed of two parts, the electronic and the phononic parts. The phonon thermal conductivity in general dominates the total thermal conductivity in semiconductors, whereas the electronic part is usually negligible. The electronic thermal conductivity κ_e, however, is proportional to the electronic conductivity. In the case of gated NWs, thus, it is important to examine how the electronic thermal conductivity changes as we largely increase the electrical conductivity of the channel. Figure 5 shows the electronic part of the thermal conductivity for the same channel cases as in Fig. 2 and Fig. 3. The trend is, as expected, very similar to that of the electrical conductivity in Fig. 2. The gated NW has significantly higher electronic thermal conductivity compared to the doped NW. What is important to observe, however, is that the value of κ_e is still very low, despite the large

increase from gating. At the carrier concentrations where the power factor peaks, around p~10^{19}/cm^3, κ_e is below 0.2 W/mK. This indicates that even after the very large improvement, the total thermal conductivity will still be dominated by the phonon part.

In the amorphous limit, the phonon part of the thermal conductivity of Si is of the order of κ_l = 1 W/mK. Using this value, one could estimate the upper bound for the *ZT* figure of merit of the gated NW channel at room temperature. This is shown in Fig. 6. The *ZT* for the gated NW peaks again around concentrations of p~10^{19}/cm^3, and reaches a value just below *ZT*~0.5. This is more than ~3x larger than the *ZT* that is achieved by the doped channel. In the doped channel case the *ZT* peaks at *ZT*~0.14 and at larger carrier concentrations of p~5x10^{19}/cm^3. Indeed, large benefits can be achieved in the figure of merit by field-effect density modulation methods, rather than direct doping.

Note that what we present in Fig. 6 is the upper bound of the *ZT* assuming amorphous thermal conductivity conditions. We have in addition calculated the phonon part of the thermal conductivity for this particular [100] NW with diameter *D*=12nm using the atomistic modified valence-force-field method (MVFF), as described in Refs [26, 27]. The value for the thermal conductivity turned out to be slightly higher κ_l = 2.5 W/mK (assuming diffusive phonon-phonon transport and diffusive phonon-boundary scattering), which could lower the maximum *ZT* to a value close to *ZT*~0.2. On the other hand, NW channels can be optimized with respect to their transport orientation [1, 22] and choosing the optimal orientation could provide higher *ZT*. In either case, however, gating rather than doping could provide ~3X improvements in the thermoelectric performance of NW channels.

Finally, in Fig. 7 we investigate the *ZT* figure of merit of the gated *D*=12nm [100] NW at elevated temperatures, as Si is known to have better thermoelectric properties at higher temperatures. In Fig. 7 we plot results for phonon-limited TE transport conditions versus carrier density. Results for temperatures 300K, 450K, 600K, and 750K are shown as indicated in the figure. The amorphous limit is still assumed for the phonon part of the thermal conductivity, which will provide an upper limit for the TE performance. From a

maximum of *ZT*~0.5 at room temperature, the *ZT* increases to *ZT*~1.2 at 750K, achieved at slightly increased carrier densities. Such a high *ZT* value holds promise for gated Si NWs as good candidates for high temperature thermoelectrics.

IV. Conclusions

In conclusion, we have investigated the effect of gating in the thermoelectric power factor and *ZT* figure of merit of narrow p-type Si [100] NWs of diameter *D*=12nm using self-consistent atomistic tight-binding calculations and Boltzmann transport. We show that gating rather than doping can significantly increase the electronic conductivity, and result in a larger than 3-fold improvement in their power factor. Surface roughness scattering is weak, and although the carriers accumulate around the nanowire surface under gating, the conductivity is not affected significantly. The electronic part of the thermal conductivity, although increased by gating, is very small to significantly play any role, and the overall thermal conductivity is still determined by the phonon part. Finally, we have shown that the *ZT* figure of merit can be improved by more than ~3x in gated channels.

Acknowledgement: The work leading to these results has received funding from the European Community's Seventh Framework Programme under grant agreement no. FP7-263306, and the Austrian Science fund FWF under project number P25368.

References

[1] N. Neophytou and H. Kosina, *Phys. Rev. B*, 83, 245305, 2011.

[2] M. Zebarjadi, G. Joshi, G. Zhu, B. Yu, A. Minnich, Y. Lan, X. Wang, M. Dresselhaus, Z. Ren, and G. Chen, *Nano Lett.*, 11, 6, pp. 2225–2230, 2011

[3] B. Yu, M. Zebarjadi, H. Wang, K. Lukas, H. Wang, D. Wang, C. Opeil, M. Dresselhaus, G. Chen, and Z. Ren, *Nano Lett.*, 12, 4, pp. 2077–2082, 2012

[4] B. M. Curtin, E. A. Codecido, S. Krämer, and J. E. Bowers, *Nano Lett.*, 13, 11, pp. 5503–5508, 2013.

[5] Y. Tian, M. R. Sakr, J. M. Kinder, D. Liang, M. J. MacDonald, R. L. J. Qiu, H.-J. Gao, and X. P. A. Gao, *Nano Lett.*, 12, 12, pp. 6492–6497, 2012.

[6] J. Moon, J.-H. Kim, Z. C.Y. Chen, J. Xiang, and R. Chen, *Nano Lett.*, 13, 3, pp. 1196–1202, 2013.

[7] B. M. Curtin and J. E. Bowers, *J. Appl. Phys.*, 115, 143704, 2014.

[8] W. Liang, A. I. Hochbaum, M. Fardy, O. Rabin, M. Zhang and P. Yang, *Nano Lett.*, 9, 4, pp. 1689–1693, 2009.

[9] A. I. Hochbaum, R. Chen, R. D. Delgado, W. Liang, E. C. Garnett, M. Najarian, A. Majumdar, and P. Yang, *Nature*, vol. 451, pp. 163-168, 2008.

[10] A.I. Boukai, Y. Bunimovich, J. T.-Kheli, J.-K. Yu, W. A. Goddard III, and J. R. Heath, *Nature*, vol. 451, pp. 168-171, 2008.

[11] N. Neophytou, O. Baumgartner, Z. Stanojevic, and H. Kosina, *Solid State Electronics*, 90, pp. 44–50, 2013.

[12] T. B. Boykin, G. Klimeck, and F. Oyafuso, *Phys. Rev. B*, vol. 69, pp. 115201-115210 (2004).

[13] G. Klimeck, S. Ahmed, H. Bae, N. Kharche, S. Clark, B. Haley, S. Lee, M. Naumov, H. Ryu, F. Saied, M. Prada, M. Korkusinski, and T. B. Boykin, *IEEE Trans. Electr. Dev.*, vol. 54, no. 9, pp. 2079-2089 (2007).

[14] N. Neophytou, M. Wagner, H. Kosina, and S. Selberherr, *Journal of Electronic Materials*, 39, 9, 1902-1908, 2010.

[15] S. Lee, F. Oyafuso, P. Von, Allmen, and G. Klimeck, *Phys. Rev. B*, vol. 69, pp. 045316-045323 (2004).

[16] G. D. Mahan and J. O. Sofo, Proc. Natl. Acad. Sci. USA, vol. 93, pp. 7436-7439 (1996).

[17] T. J. Scheidemantel, C. A.-Draxl, T. Thonhauser, J. V. Badding, and J. O. Sofo, *Phys. Rev. B*, vol. 68, p. 125210 (2003).

[18] S. Jin, M. V. Fischetti, and T.-W. Tang, *J. Appl. Phys.*, 102, 083715 (2007).

[19] H. Sakaki, T. Noda, K. Hirakawa, M. Tanaka, and T. Matsusue, *Appl. Phys. Lett.*, vol. 51, no. 23, p. 1934 (1987).

[20] K. Uchida and S. Takagi, *Appl. Phys. Lett.*, vol. 82, no. 17, pp. 2916-2918 (2003).

[21] E. B. Ramayya, D. Vasileska, S. M. Goodnick, and I. Knezevic, *J. Appl. Phys.*, vol. 104, p. 063711 (2008).

[22] N. Neophytou and H. Kosina, *Phys. Rev. B*, 84, 085313, 2011.

[23] H. J. Ryu, Z. Aksamija, D. M. Paskiewicz, S. A. Scott, M. G. Lagally, I. Knezevic, and M. A. Eriksson, Phys. Rev. Lett. 105, 256601, 2010

[24] N. Neophytou and H. Kosina, J. Appl. Phys., 112, 024305, 2012.

[25] K. Rameshan, N. A. Wong, K. Chan, S. P. Sim, C. Y. Yang, *Solid-State Electronics*, 46, 153-156, 2002.

[26] H. Karamitaheri, N. Neophytou, and H. Kosina, *Journal of Electronic Materials*, 43, 1829, 2014.

[27] H. Karamitaheri, N. Neophytou, and H. Kosina, *J. Appl. Phys.*, 115, 024302, 2014.

Figure 1:

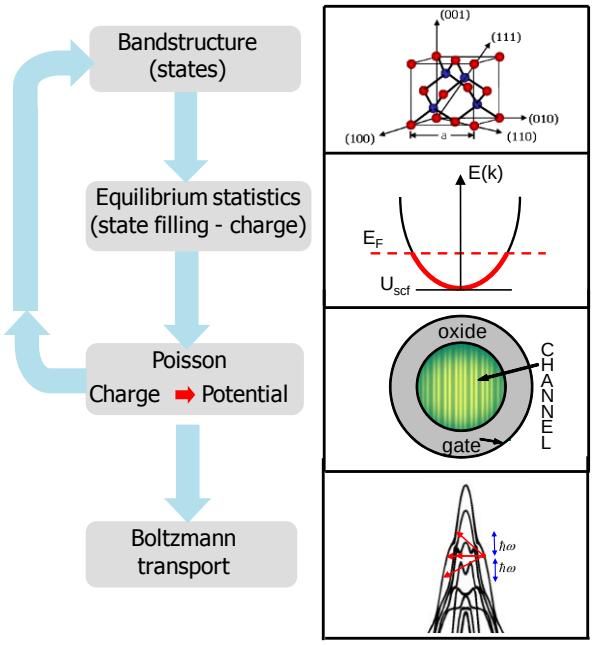

Figure 1 caption:

Simulation procedure steps (from top to bottom). The NW bandstructure is calculated using the $sp^3d^5s^*$ tight-binding model. (b) Equilibrium statistics are used to calculate the charge distribution in the NW. (c) The charge is self-consistently coupled to a 2D Poisson equation to obtain the electrostatic potential in the cross section of the wire. (d) Upon convergence, Boltzmann transport theory is used for mobility calculations. (Examples of relevant valence band scattering mechanisms are shown.)

Figure 2:

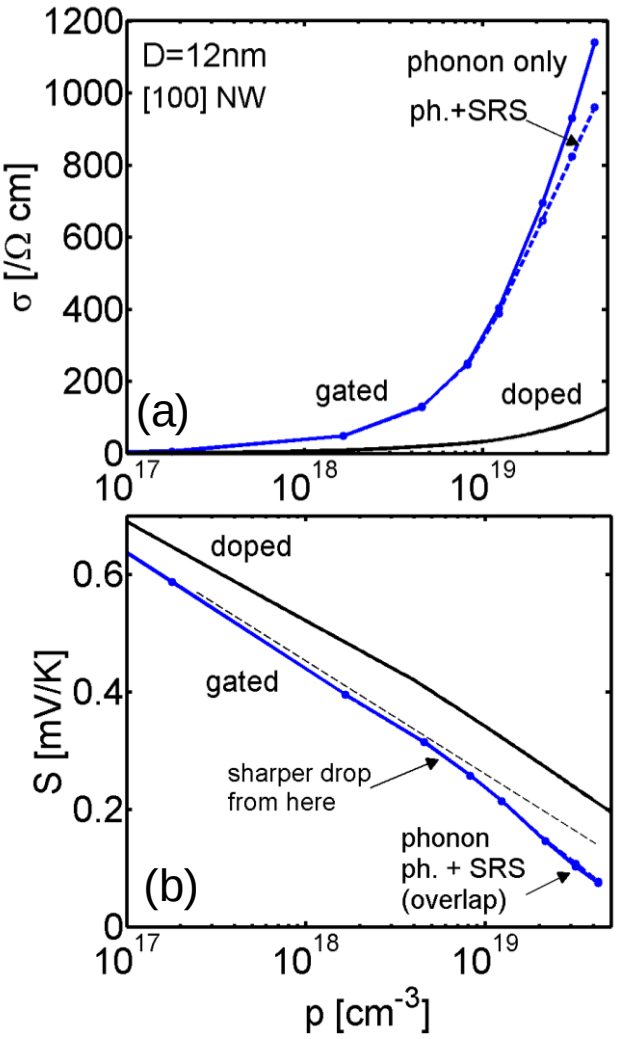

Figure 2 caption:

Thermoelectric coefficients for the *D*=12nm [100] NW versus carrier density under three different channel situations: (i) Gated NW under phonon scattering-limited considerations (blue-dot-solid line). (ii) Gated NW under phonon scattering and SRS considerations (blue-dot-dashed line). (iii) Doped (non-gated) NW under phonon scattering, IIS, and SRS considerations (black-solid line). (a) The electrical conductivity. (b) The Seebeck coefficient. Straight dashed line is guide of the eye.

Figure 3:

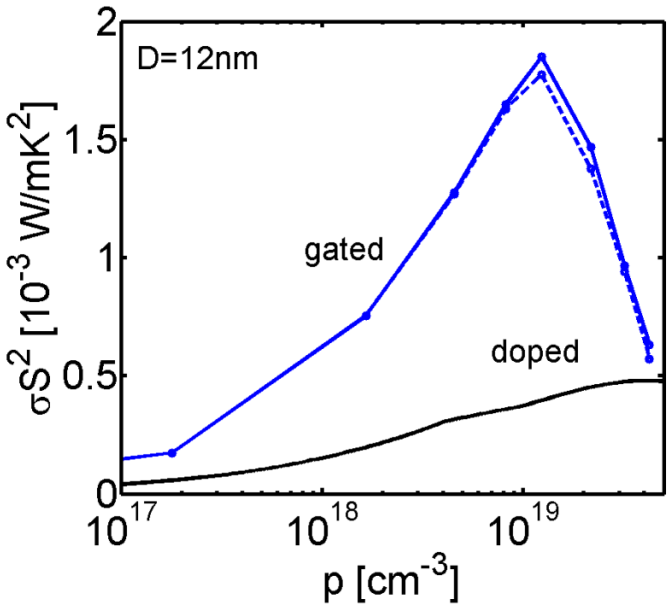

Figure 3 caption:

The thermoelectric power factor of the *D*=12nm [100] NW versus carrier density under three different channel situations: (i) Gated NW under phonon scattering-limited considerations (blue-dot-solid line). (ii) Gated NW under phonon scattering and SRS considerations (blue-dot-dashed line). (iii) Doped (non-gated) NW under phonon scattering, IIS, and SRS considerations (black-solid line).

Figure 4:

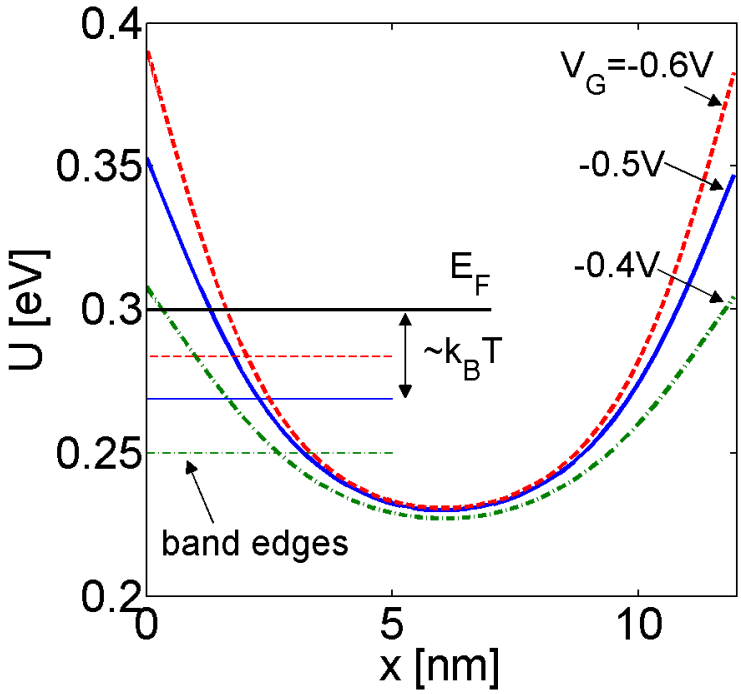

Figure 4 caption:

The electrostatic potential energy profile along the diameter of the D=12nm nanowire. Three cases are shown: i) Gate bias V_G=-0.4V (green-dashed-dot line), ii) Gate bias V_G=-0.5V (blue-solid line), which is the one that provides the maximum power factor, and iii) i) Gate bias V_G=-0.6V (red-dashed line). The valence band edges for the three cases are indicated by the same line types. The Fermi level E_F is depicted by the black line.

Figure 5:

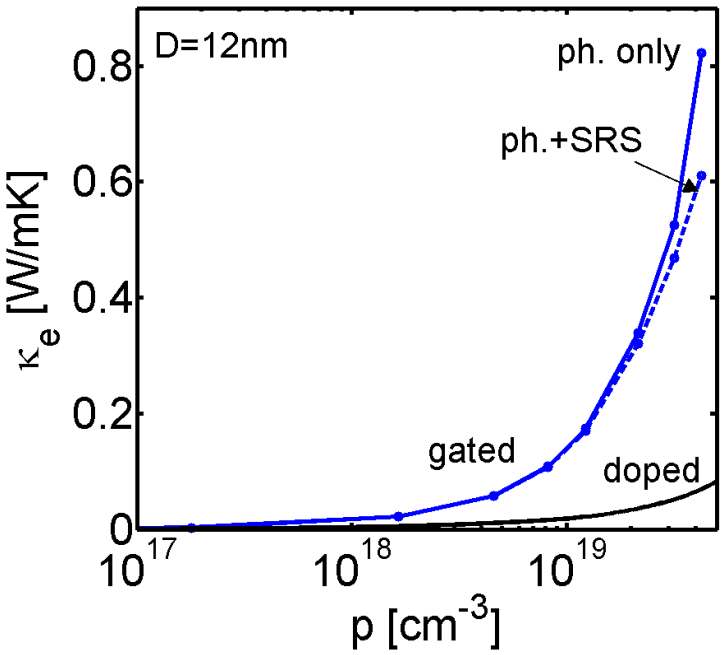

Figure 5 caption:

The electronic part of the thermal conductivity of the *D*=12nm [100] NW versus carrier density under three different channel situations: (i) Gated NW under phonon scattering-limited considerations (blue-dot-solid line). (ii) Gated NW under phonon scattering and SRS considerations (blue-dot-dashed line). (iii) Doped (non-gated) NW under phonon scattering, IIS, and SRS considerations (black-solid line).

Figure 6:

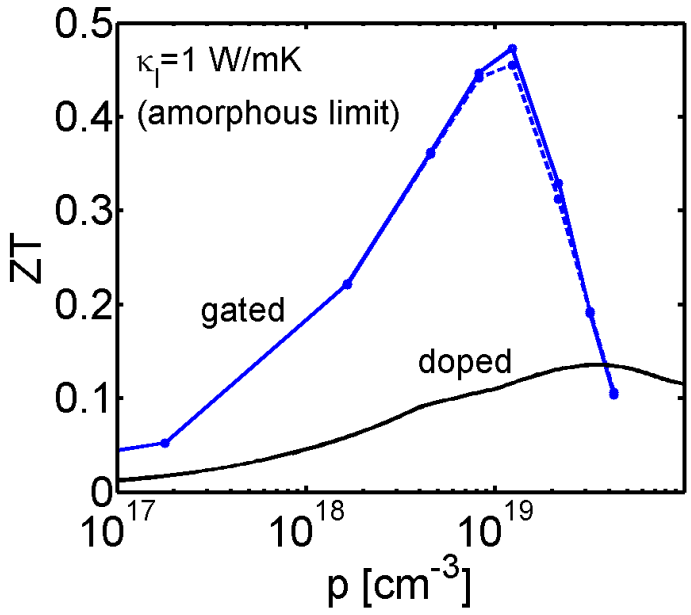

Figure 6 caption:

The *ZT* figure of merit of the *D*=12nm [100] NW versus carrier density under three different channel situations: (i) Gated NW under phonon scattering-limited considerations (blue-dot-solid line). (ii) Gated NW under phonon scattering and SRS considerations (blue-dot-dashed line). (iii) Doped (non-gated) NW under phonon scattering, IIS, and SRS considerations (black-solid line). The amorphous limit is assumed for the phonon part of the thermal conductivity.

Figure 7:

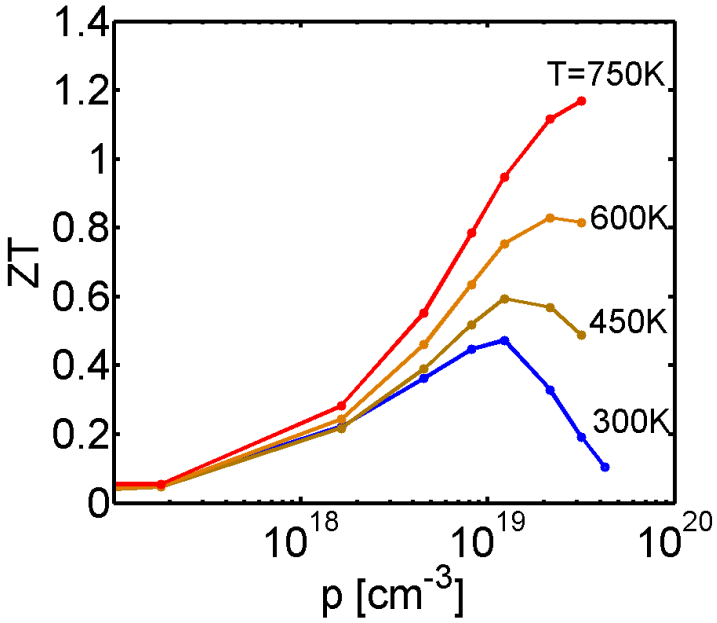

Figure 7 caption:

The *ZT* figure of merit of the gated *D*=12nm [100] NW versus carrier density under phonon-limited transport conditions versus carrier density. Results for temperatures 300K, 450K, 600K, and 750K are shown as indicated in the figure. The amorphous limit is assumed for the phonon part of the thermal conductivity.